Modelling groundwater contamination above a nuclear waste repository at Gorleben, Germany

Michael O. Schwartz

Abstract The candidate repository for high-level nuclear waste in the Gorleben salt dome, Germany, is expected to host 8,550 tonnes of uranium in burnt fuel. It has been proposed that 5,440 waste containers be deposited at a depth of about 800m. There is 260–280m of siliciclastic cover sediments above the proposed repository. The potential groundwater contamination in the siliciclastic aquifer is simulated with the TOUGHREACT and TOUGH2-MP codes for a three-dimensional model with 290,435 elements. Two deterministic cases are simulated. The single-phase case considers the transport of radionuclides in the liquid phase only. The two-phase case accounts for hydrogen gas generated by the corrosion of waste containers and release of gaseous C-14. The gas release via a backfilled shaft is assumed to be steady (non-explosive). The simulation period is 2,000,000 years for the single-phase case and 7,000 years for the two-phase case. Only the radioactive dose in the two-phase case is higher than the regulatory limit (0.1mSv/a).

Keywords Groundwater contamination · Numerical modeling · Radioactive waste · Germany

Introduction

The candidate repository for high-level nuclear waste in the Gorleben salt dome, Germany, is the only one of its kind. There are medium-level repositories in rock salt, but nowhere else in the world is a high-level repository planned. Ever since the start of the exploration in 1979, the potential groundwater contamination associated with the Gorleben project has been a much debated issue. The Gorleben site is as controversial as the Yucca Mountain site in the USA, which is also characterised by a high-salinity hydrochemical regime, albeit for different reasons (arid climate). As a consequence of the political debates, the Gorleben project was halted during the moratorium from 2000 to 2010 and the Yucca Mountain project was stopped in 2011. Less controversial are candidate repositories with a low-salinity hydrochemical regime in granite (SKB 2006; Nykyri et al. 2008) or clay (NAGRA 2002).

It is difficult to predict the post-moratorium activities at Gorleben. The governmental Ethikkommison Sichere Energieversorgung (the German Ethics Commission on Safe Energy Supply) published its final report on 30 May 2011. The commission recommended that nuclear waste be deposited in such a manner that future generations will be capable of extracting the waste and that alternative host rocks be investigated. A repository in salt such as the Gorleben site, offers relatively unfavourable conditions for extracting deposited waste in comparison to repositories in granite or clay. Possibly, mine development will not continue at the Gorleben site and the activities will be scaled down to pure exploration.

During the 10-year Gorleben moratorium, there was no underground exploration or development but care-and-maintenance and scientific research has continued. The publication of a three-volume monograph is the most important scientific activity of the moratorium period (Klinge et al. 2007; Köthe et al. 2007; Bornemann et al. 2008). The monograph synthesises the work performed from 1979 to 2000. Another review of the pre-moratorium period is presented by Ludwig et al. (2001). Two variable-salinity flow simulations but no contaminant-transport simulations were performed prior to the moratorium. Vogel and Schelkes (1996) calculated the variable-salinity flow in two dimensions but the ambitious project of modelling the whole of the 350 km^2 Gorleben exploration area (Klemenz et al. 1998; Ludwig et al. 2001) was never completed. Only the first test run for a small part of the exploration area is documented: "Because of the potential restrictions of the software and hardware, a generic and simplified model based on the characteristics of the Gorleben site was set up. The aim of this model was to gain experience in simulating fully coupled groundwater flow and salt transport at the regional scale in three dimensions as well as to study the variable-density spatial

Received: 22 May 2011 / Accepted: 16 December 2011
Published online: 17 January 2012

© Springer-Verlag 2012

M. O. Schwartz (✉)
MathGeol,
Postfach 101204, 30833 Langenhagen, Germany
e-mail: mathgeol@yahoo.de
Tel.: +49-152-05910263
Fax: +49-152-0505910263

 DOI 10.1007/s10040-011-0825-z

distribution and its influence on the groundwater movement" (Klemenz et al. 1998). "But, nevertheless, even this model is far from a realistic groundwater flow field" (Ludwig et al. 2001).

During the moratorium, Keesmann et al. (2005) calculated the contaminant transport in a variable-salinity model with two dimensions and Vogel (2005) calculated the contaminant transport in an idealised zero-salinity model with three dimensions. In contrast to the pre-moratorium activities, the simulations performed during the moratorium did not fully exploit the possibilities of the available computing technology.

Apart from the Gorleben models, there are several benchmark calculations of the two-dimensional (2D) flow in an aquifer above a salt dome (Oldenburg and Pruess 1995a, b; Oldenburg et al. 1996; Johns and Rivera 1996; Konikow et al. 1997). Three-dimensional (3D) cases have been calculated for the existing medium-level repository Asse 2, Germany. GSF (2006) simulated the transport of a non-sorbing, non-decaying tracer in a 3.2 km^2 model area. Schwartz (2009, 2010) used a smaller model area (1.8 km^2) but considered sorption and radioactive decay of parent and daughter radionuclides as well as two-phase flow (liquid and gas); the model was relatively easy to calibrate because of the relatively small size of the model area.

Despite decades of research at the Gorleben site, no realistic contaminant-transport model has been set up, i.e. a model that simulates the contaminant-transport in three dimensions and considers gas-phase and liquid-phase transport as well as variable salinity. Such a model is a prerequisite for a safety analysis even if it can only be a deterministic model with a sensitivity analysis but not a probabilistic model at the present stage of computing technology. The objective of the present study is to fill this scientific gap.

Study area

Geology

The salt, which now constitutes the Gorleben salt dome, was deposited in the Zechstein (Köthe et al. 2007). Most of the diapiric rise of the salt took place in the Cretaceous. At the beginning of the Tertiary, the salt dome already attained a shape similar to its present outline (Fig. 1). The diapiric rise was accompanied by the formation of rim synclines, where 1,000–3,000 m thick Mesozoic sediments were deposited. Apart from a few Cretaceous remnants, all Mesozoic sediments, which originally were present on top of the salt dome, have been eroded.

The Tertiary sedimentation was strongly influenced by the halokinetic process. The thickness of the siliciclastic sediments increases with increasing distance from the long axis of the salt-dome structure. In the rim synclines at both sides of the structure, the typical sequence of upper Paleocene through Miocene was deposited. Like elsewhere in north-west Germany, there is a hiatus of 1–2 million years between the deposition of the Paleocene and Eocene sediments.

The Paleocene and Eocene sediments are present as a more or less continuous layer on top of the salt dome. The thickness varies in a wide range (10–110 m). This is due to the uplift of the salt dome, subrosion as well as erosion during the Quaternary and, to lesser degree, erosion during the Tertiary. There are sporadic occurrences of lower Oligocene strata on top of the salt dome but the upper Oligocene through Miocene is completely missing except for some occurrences north of the Elbe River. In contrast, the upper Oligocene through Miocene strata in the rim synclines attained a great thickness (up to 350 m).

The Tertiary rocks are overlain by Quaternary deposits with a hiatus of 14 million years in between. In contrast to the depositional conditions during the Tertiary, the distribution of the Quaternary deposits is not influenced by halokinetic processes but by exaration, accumulation and glacial-tectonic events during the north-European glacial epoch. The base of the Quaternary lies between 20 m and 300 m below the present land surface. The oldest Quaternary deposits are fluviatile sands of the Menapian glacial stage—1,200,000–1,070,000 years (a) before present (BP)—which are overlain by the Bavel-Cromer-Complex interglacial (1,070,000–480,000 a BP). These deposits fill a small paleo-depression south-west of shaft 1 (Fig. 1). A much larger structure is the Gorlebener Rinne, which forms an acute angle (<50°) with the long axis of the salt dome. This paleo-channel was created by erosional processes during the Elsterian glacial stage and is filled with Elsterian deposits (480,000–370,000 a BP) apart from sporadic occurrences of sediments of the Holsteinian interglacial stage (370,000–350,000 a BP). The deposits of the following Saale glacial stage (350,000–128,000 a BP) are not restricted to paleo-channels but are widely spread over the exploration area. The Eemian interglacial stage (128,000–117,000 a BP) is practically absent but sands of the Weichselian glacial stage (117,000–11,600 a BP) and the Holocene (<11,600 a BP) are widely spread.

The repository

The current model scenarios assume that the repository will accommodate 5,440 waste containers with a total of 8,550 tonnes of uranium (U) in burnt fuel (Keesmann et al. 2005). The waste containers, which are made of Mn–Ni steel, have a length of 5.5 m and a diameter of 1.6 m (Javeri 2006). The proposal is that they will be emplaced in horizontal disposal drifts, which will be connected to two shafts by a system of access drifts. The envisaged disposal depth is about 800 m. There are 260–280 m Quaternary-Tertiary siliciclastic sediments above the present mine workings within the Zechstein salt dome (area between shaft 1 and shaft 2; Fig. 1).

Model set-up

Geometry of the models

The geometry of the irregular rectangular mesh is defined by the interface I_{ij}, the area F_{ij} of the interface, the neighbouring nodes N_i and N_j, the distance $d1_{ij}$ and $d2_{ij}$

 DOI 10.1007/s10040-011-0825-z

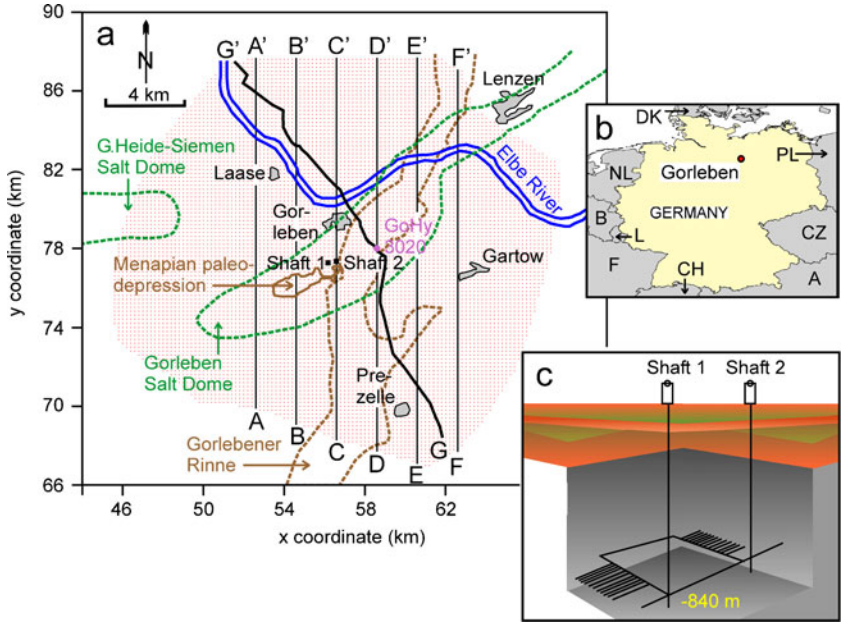

Fig. 1 **a–b** Maps of the Gorleben model area with outline of the salt domes at −800 m depth (*dashed green line*), outline of the Menapian paleo-depression at −125 m depth (*solid brown line*), Gorlebener Rinne at −150 m depth (*dashed brown line*), villages/small towns (in *grey*), model mesh (in *red*) and traces of sections (*AA'*, *BB'*, etc; see Figs. 6 and 8). **c** Diagram of the repository layout. *A* Austria, *B* Belgium, *CH* Switzerland, *CZ* Czech Republic, *DK* Denmark, *F* France, *L* Luxembourg, *NL* Netherlands, *PL* Poland

between interface and node N_i and N_j, respectively, as well as the angle between the gravitational acceleration vector and the line connecting the nodes N_i and N_j. An element volume without any specific shape is associated with each node.

The mesh has 290,435 nodes and measures 22,400 m× 21,000 m×400 m (Figs. 1 and 2; Table 1). Three sets of nodal distances (sums of $d1_{ij}$ and $d2_{ij}$) in the x and y direction are used. The backfilled shaft 2, which measures 6×6 m horizontally, and the area immediately surrounding shaft 2 (shaft wall and bedrock) have horizontal nodal distances of 2 m. An intermediate zone (only bedrock) has horizontal nodal distances of 20 m. The remaining part of the primary mesh (only bedrock) has nodal distances of 200 m.

The top layer has nodal z values representing the freshwater head (between 12.7 and 22.1 m elevation above sea level), the piezometric bottom being at ±0 m elevation (Fig. 3). The second layer has nodes located 0.1 m vertically below those of the top layer. The vertical nodal distance between the following 32 layers is 12.5 m. The top layer, which serves to maintain constant pressure (10^5 Pa) and salinity, exclusively consists of infinite-volume boundary elements (10^{45} m^3). The thermodynamic conditions of these boundary elements do not change at all. Thus, Dirichlet conditions are implemented at the boundary between the topmost and second topmost layer.

The head is fixed in all simulations except for a sensitivity test with case C (see section Sensitivity analysis in the following). The head changes from simulation year zero (12.7–22.1 m) to year 100,000 (8.0–22.1 m) and year 200,000 (3.3–22.1 m) in case C; this corresponds to an increase of the hydraulic gradient by a factor of 1.5 and 2, respectively. The transient head conditions are translated into transient mesh geometries, i. e., the z-values of the top layer change according to the data of Fig. 3. These changes account for a possible drop of the sea level and increase of erosion rates. A more advanced sensitivity analysis would consider a further increase of the hydraulic gradient. However, the necessary modifications of the mesh geometry would be beyond the scope of this report.

Other boundary cells are the rock-salt cells and the bottom-layer cells of the −375-m level. They have a volume of 10^{14} m^3. This volume is large enough for maintaining nearly constant salinity throughout the simulation period but is simultaneously flexible enough to account for pressure adjustments. The volume of the remaining cells is calculated according to their nodal positions. A secondary boundary cell is connected to the primary cell in the centre of shaft 2 at the top of the salt dome (−237.5-m level). The volume (100 m^3) of the secondary cell, which is used for injecting HCO_3^-, has been determined by trial-and-error (see section Methodology in the following).

Hydrostratigraphy and hydraulic properties

The hydrostratigraphic information of 197 drill-hole logs is transferred to the nearest model node at the corresponding z-position (Figs. 3 and 4; Ludwig et al. 1989; Beushausen and Ludwig 1990; Ludwig et al. 1993; Klinge et al. 2001). Based on this information, the hydrostratigraphic units for the remaining nodes are assigned by interpolation and extrapolation.

All simulations are performed with the hydraulic properties of the hydrostratigraphic units of the caprock and cover sediments of case 1 (Figs. 5 and 6; Table 2)

 DOI 10.1007/s10040-011-0825-z

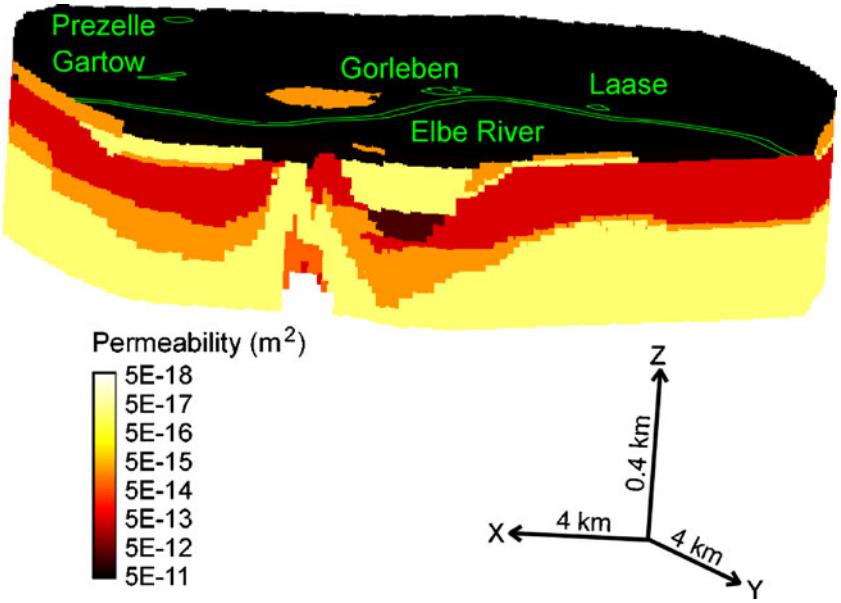

Fig. 2 Gorleben model. Block diagram representing permeability: vertical exaggeration ratio 12:1. *Green lines* = topographic features (see Fig. 1)

according to Vogel (2005). This scheme is based on the geometric mean of empirical maximum and minimum values. Three additional data sets (cases 2, 3 and 4; Table 2) were tested but were found to yield unsatisfactory results in terms of salinity distribution (see Methodology). Case 2 is based on permeability ranges for Quaternary-Tertiary units used by Vogel and Schelkes (1996), case 3 is based on Keesmann et al. (2005) and case 4 is based on Klemenz et al. (1998). The backfill of shaft 2 has a permeability of 10^{-12} m^2 and a porosity of 0.3 (base case; Table 3). These are arbitrary model assumptions taken from Javeri (2006).

Sorption and diffusion

The linear distribution coefficients for the radionuclides in the one-phase scenario are taken from Suter et al. (1998). C-14 in the two-phase scenario is assumed to be non-sorbing under low oxygen fugacities compatible with the release of hydrogen gas. There is a considerable uncertainty with respect to the effective diffusivity in porous media (Saripalli et al. 2002) and simplifying assumptions are justified. The effective diffusivity is derived from a free-water diffusivity of 2×10^{-9} m^2/s for anions and neutral species and 1×10^{-9} m^2/s for cations. These values are multiplied by a formation factor, which is 0.5 for anions and neutral species and unity for cations. The formation factor accounts for both the diffusive resistances offered by the porous medium and surface diffusion.

Boundary conditions

The infinite-volume elements (10^{45} m^3) of the top layer, which impose Dirichlet conditions, have a pressure of 10^5 Pa and zero salinity. The large volume elements of the rock-salt cells and the bottom layer (10^{14} m^3) impose nearly Dirichlet conditions with respect to salinity (0.25 mass fraction salt; see Methodology) but allow flexible pressure adjustments. The outer lateral boundaries are closed. Open lateral boundaries (boundary element volume $>10^6$ m^3) are less suitable for maintaining salinity gradients close to present values (see Methodology).

Time-dependent Neumann boundary conditions are imposed at the borehole location GoHy3020 on the −250-m level in the one-phase scenario as well as at the primary central cell of shaft 2 on the −237.5-m level and a secondary boundary cell that is connected to this primary cell in the two-phase scenario. The injection rates are published near-field releases, i.e., releases according to the hydrochemical regime of the backfilled underground workings in the salt dome. This study only simulates the far field, i.e. the hydrochemical regime of the caprock and cover sediments. The far field simulations use the near-field data as input.

To date, only two near-field scenarios have been published. The first considers a single-phase case with liquid-phase transport only. The second considers a two-phase case with both liquid-phase and gas-phase transport. The near-field release of the single-phase scenario (Figs. 7a–c; Keesmann et al. 2005) is the latest update of the Early-Intrusion-Case of Storck et al. (1988). Brine is assumed to be released from brine pockets in the salt dome immediately after the closure of the repository. One hundred years later, brine originating from the siliciclastic aquifer above the salt dome intrudes the disposal drifts. The brines cause the corrosion of the waste canisters. In the year 500, the canisters loose their transport resistance, and the brines start dissolving the radionuclides up to the solubility limits specified in Table 1. The mobilisation rate is 1.0×10^{-6} a^{-1} and 3.6×10^{-3} a^{-1} for the fuel matrix and metal components, respectively. The brines are squeezed out of the repository due to the compaction of the elastically deforming rock salt according to the rates shown in Fig. 7c. The exit point of the contaminated brines is the contact between Quaternary sediments and

 DOI 10.1007/s10040-011-0825-z

Table 1 Set-up of the Gorleben model

General properties	
Model length/width/height (m)	22,400/21,000/400
Model temperature (°C)	25
Simulation period (a)	2,000,000
Rock density (kg/m^3)	2,500
Saturated hydraulic properties (see also Table 2)	
Permeability (m^2)	5×10^{-11}–1×10^{-18}
Porosity (−)	0.03–0.3
Unsaturated hydraulic properties	
Residual liquid saturation	0.
Residual gas saturation	0.
Van Genuchten parameter α (Pa)	4.46×10^{4}
Van Genuchten parameter m (−)	0.21
Inventory of radionuclides after 10 years of cooling	
Am-241 (total/fuel)[a] (Bq)	1.7×10^{18}/1.7×10^{18}
C-14 (total/fuel)[a] (Bq)	1.6×10^{14}/4.2×10^{13}
Cl-36 (total/fuel)[a] (Bq)	2.9×10^{12}/2.7×10^{12}
Cs-135 (total/fuel) [a] (Bq)	1.9×10^{14}/1.8×10^{14}
I-129 (total/fuel)[a] (Bq)	1.7×10^{13}/1.6×10^{13}
Ni-59 (total/fuel)[a] (Bq)	5.1×10^{14}/2.4×10^{12}
Np-237 (total/fuel)[a] (Bq)	1.2×10^{14}/1.2×10^{14}
Pa-231 (total/fuel)[a] (Bq)	1.1×10^{10}/1.1×10^{10}
Pu-239 (total/fuel)[a] (Bq)	1.9×10^{17}/1.9×10^{17}
Pu-240 (total/fuel)[a] (Bq)	4.4×10^{17}/4.4×10^{17}
Pu-242 (total/fuel)[a] (Bq)	3.2×10^{15}/3.2×10^{15}
Ra-226 (total/fuel)[a] (Bq)	9.0×10^{7}/9.0×10^{7}
Se-79 (total/fuel)[a] (Bq)	1.5×10^{14}/1.4×10^{14}
Tc-99 (total/fuel)[a] (Bq)	2.2×10^{15}/2.2×10^{15}
Th-229 (total/fuel)[a] (Bq)	5.5×10^{7}/5.5×10^{7}
Th-230 (total/fuel)[a] (Bq)	3.4×10^{10}/3.4×10^{10}
U-233 (total/fuel)[a] (Bq)	3.1×10^{10}/3.1×10^{10}
U-235 (total/fuel)[a] (Bq)	4.3×10^{12}/4.3×10^{12}
U-236 (total/fuel)[a] (Bq)	7.2×10^{13}/7.2×10^{13}
U-238 (total/fuel)[a] (Bq)	1.0×10^{14}/1.0×10^{14}
Half-life of radionuclides	
Am-241 (a)[b]	432
C-14 (a)	5,700
Cl-36 (a)	3.0×10^{5}
Cs-135 (a)	2.0×10^{6}
I-129 (a)	1.6×10^{7}
Ni-59 (a)	7.5×10^{4}
Np-237 (a)	2.1×10^{6}
Pa-231 (a)	3.3×10^{4}
Pu-239 (a)[b]	2.4×10^{4}
Pu-240 (a)[b]	6.5×10^{3}
Pu-242 (a)[b]	3.7×10^{5}
Ra-226 (a)	1.6×10^{3}
Se-79 (a)	1.1×10^{6}
Tc-99 (a)	2.1×10^{5}
Th-229 (a)	7.9×10^{3}
Th-230 (a)[b]	7.5×10^{4}
U-233 (a)	1.6×10^{5}
U-235 (a)	7.0×10^{8}
U-236 (a)	2.3×10^{7}
U-238 (a)	4.5×10^{9}
Distribution coefficients for low-salinity water (≤10 g/L salt) in the one-phase scenario	
Am (sand/silt-clay) (L/kg)	300/20,000
C (sand/silt-clay) (L/kg)	0.2/2
Cl (sand/silt-clay) (L/kg)	0.1/0.1
Cs (sand/silt-clay) (L/kg)	70/400
I (sand/silt-clay) (L/kg)	2/2
Ni (sand/silt-clay) (L/kg)	20/300
Np (sand/silt-clay) (L/kg)	10/300
Pa (sand/silt-clay) (L/kg)	600/6,000
Pu (sand/silt-clay) (L/kg)	100/3,000
Ra (sand/silt-clay) (L/kg)	40/300
Se (sand/silt-clay) (L/kg)	1/1
Tc (sand/silt-clay) (L/kg)	1/6
Th (sand/silt-clay) (L/kg)	200/2,000
U (sand/silt-clay) (L/kg)	2/80
Distribution coefficients for high-salinity water (>10 g/L salt) in the one-phase scenario	
Am (sand/silt-clay) (L/kg)	3,000/20,000
C (sand/silt-clay) (L/kg)	0.2/2
Cl (sand/silt-clay) (L/kg)	0.1/0.1
Cs (sand/silt-clay) (L/kg)	2/70
I (sand/silt-clay) (L/kg)	0.1/2
Ni (sand/silt-clay) (L/kg)	6/90
Np (sand/silt-clay) (L/kg)	10/300
Pa (sand/silt-clay) (L/kg)	600/6,000
Pu (sand/silt-clay) (L/kg)	100/3,000
Ra (sand/silt-clay) (L/kg)	2/40
Se (sand/silt-clay) (L/kg)	1/1
Tc (sand/silt-clay) (L/kg)	1/1
Th (sand/silt-clay) (L/kg)	200/200
U (sand/silt-clay) (L/kg)	0.6/20
Distribution coefficients for the two-phase scenario	
C (sand/silt-clay) (L/kg)	0/0
Aqueous phase diffusivity	
Salt (m^2/s)	1.0×10^{-7}
Hydrogen (m^2/s)	1.0×10^{-9}
All radionuclides (m^2/s)	1.0×10^{-9}
Liquid-phase solubility in the one-phase scenario	
Am (mol/L)	1.0×10^{-5}
C (mol/L)	1.0×10^{-2}
Cl (mol/L)	Unlimited
Cs (mol/L)	Unlimited
I (mol/L)	Unlimited
Ni (mol/L)	1.0×10^{-4}
Np (mol/L)	1.0×10^{-5}
Pa (mol/L)	1.0×10^{-6}
Pu (mol/L)	1.0×10^{-6}
Ra (mol/L)	1.0×10^{-6}
Se (mol/L)	1.0×10^{-4}
Tc (mol/L)	1.0×10^{-4}
Th (mol/L)	1.0×10^{-6}
U (mol/L)	1.0×10^{-4}
Liquid-phase solubility in the two-phase scenario	
C (mol/L)	Unlimited
Dose conversion factor (DCF)	
Am-241 (Sv/a:Bq/L)	8.0×10^{-4}
C-14 (Sv/a:Bq/L)	4.6×10^{-5}
Cl-36 (Sv/a:Bq/L)	3.5×10^{-5}
Cs-135 (Sv/a:Bq/L)	5.7×10^{-5}
I-129 (Sv/a:Bq/L)	5.6×10^{-4}
Ni-59 (Sv/a:Bq/L)	4.9×10^{-6}
Np-237 (Sv/a:Bq/L)	4.7×10^{-3}
Pa-231 (Sv/a:Bq/L)	4.0×10^{-2}
Pu-239 (Sv/a:Bq/L)	9.8×10^{-4}
Pu-240 (Sv/a:Bq/L)	9.6×10^{-4}
Pu-242 (Sv/a:Bq/L)	9.4×10^{-4}
Ra-226 (Sv/a:Bq/L)	3.0×10^{-2}
Se-79 (Sv/a:Bq/L)	3.4×10^{-4}
Tc-99 (Sv/a:Bq/L)	8.8×10^{-6}
Th-229 (Sv/a:Bq/L)	1.7×10^{-2}
Th-230 (Sv/a:Bq/L)	3.7×10^{-2}
U-233 (Sv/a:Bq/L)	3.9×10^{-3}
U-235 (Sv/a:Bq/L)	3.3×10^{-3}
U-236 (Sv/a:Bq/L)	5.6×10^{-4}
U-238 (Sv/a:Bq/L)	7.1×10^{-4}

[a] The difference between total activity and fuel activity is the activity of the metal components

[b] Am-241, Pu-239, Pu-240, Pu-242 and Th-230 are the parent radionuclides for Np-237, U-235, U-236, U-238 and Ra-226, respectively

 DOI 10.1007/s10040-011-0825-z

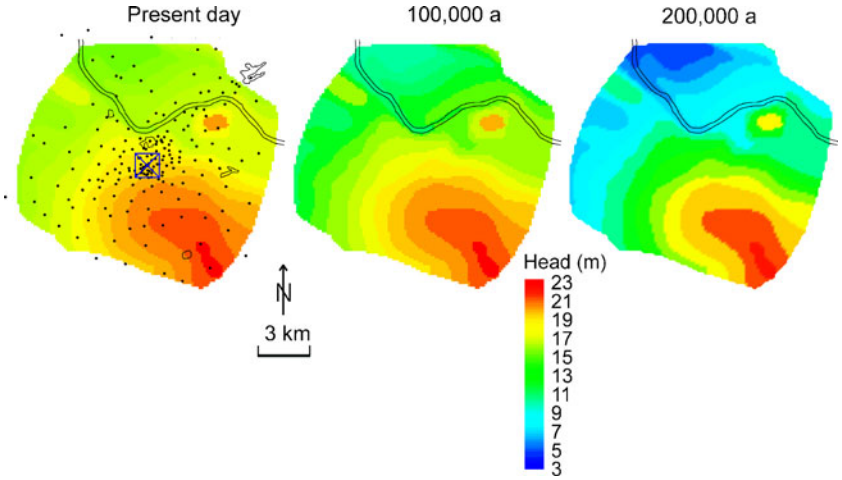

Fig. 3 Gorleben model. Head (m) in the simulation year zero (present day), 100,000 and 200,000. The location of Shaft 2 (*green cross surrounded by a green square*), boreholes (*solid black circles*) and other topographic features (*black lines* for Elbe River and villages/small towns; see Fig. 1) are also shown

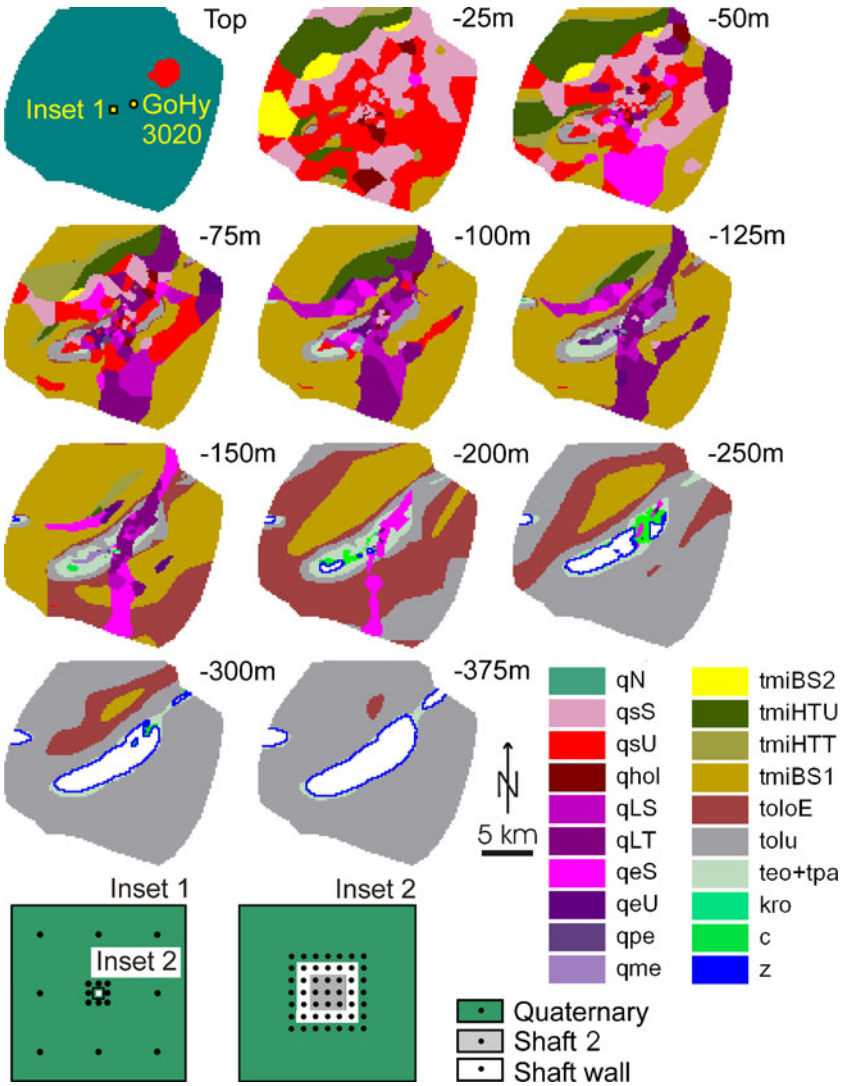

Fig. 4 Gorleben model. Hydrostratigraphic units (see Table 2) of the top layer and layers at −25, −50, −75, −100, −125, −150, −200, −250, −300 and −375 m. The location of the borehole *GoHy3020* and the structure of the model mesh in the area surrounding *shaft 2* (*Insets 1* and *2*) are also shown

 DOI 10.1007/s10040-011-0825-z

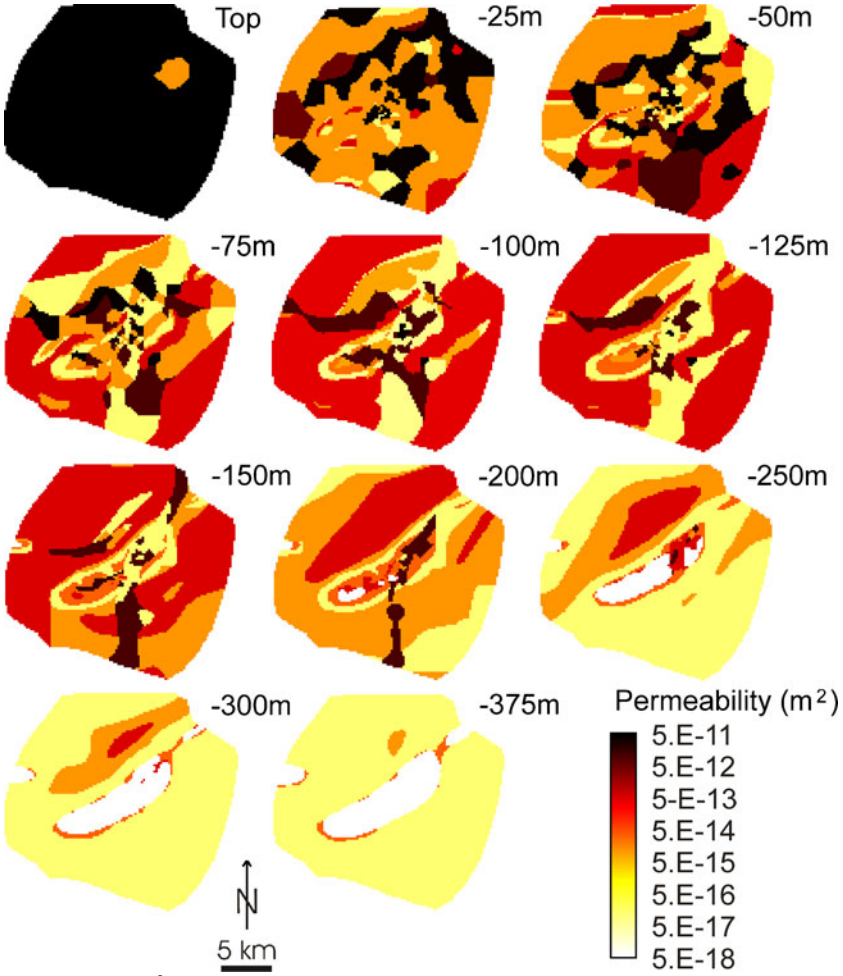

Fig. 5 Gorleben model. Permeability (m^2) of the top layer and layers at −25, −50, −75, −100, −125, −150, −200, −250, −300 and −375 m

the main anhydrite (Hauptanhydrit) layer of the Zechstein salt dome at the borehole location GoHy3020 (Fig. 4) on the −250-m level.

The two-phase scenario for the release of C-14 in the presence of a gas phase is based on a case described by Javeri (2006). Brine squeezed out from a 1,000 m^3 brine pocket is assumed to intrude a disposal drift during 2,000 years following the closure of the repository. A total of 33 waste casks is emplaced in the drift. "It is assumed that the repository is back-filled and sealed immediately after emplacement of spent fuel elements. The region separating the main undisturbed rock salt from the drift is sealed with a relatively low-permeability material comparable to the excavation-damaged zone. The shaft is backfilled with a rather permeable material like gravel sand. It is postulated that from the very beginning the whole system except the drift is fully flooded and the drift is partly flooded with saturated salt water, which can react with radioactive waste" (Javeri 2006).

At low oxygen fugacities, the container wall is subjected to corrosion dominated by the reaction

$$3Fe + 4H_2O = Fe_3O_4 + 4H_2. \quad (1)$$

The corrosion process releases hydrogen gas at a rate that increases from zero to 3.84 kg/a in the period from year zero to year 100 and decreases from 3.84 kg/a to zero in the period from year 20,000 to year 40,000. The hydrogen gas leaves the repository via the backfilled shaft according to the release rates shown in Figure 7d.

Together with hydrogen, C-14 species are released. The average waste canister contains C-14 with an activity of 3×10^{10} Bq (Keesmann et al. 2005). A fraction of 15% is available for rapid release upon failure of the canister (NAGRA 2002). This is assumed to result in a release of 13% of the initial C-14 inventory out of the repository during a 100-year period starting in the year 1,000 after the closure of the repository. The corresponding release from the total of the 33 waste containers is 1.3×10^{9} Bq/a. C-14 is the only radionuclide considered in the two-phase scenario because it is the only long-lived radionuclide that strongly partitions into the gas phase.

Computer codes

One-phase and two-phase scenarios are simulated. The TOUGHREACT code (Xu et al. 2005) is used for the two-phase scenarios. The numerical simulation program calculates chemically reactive non-isothermal flows of

 DOI 10.1007/s10040-011-0825-z

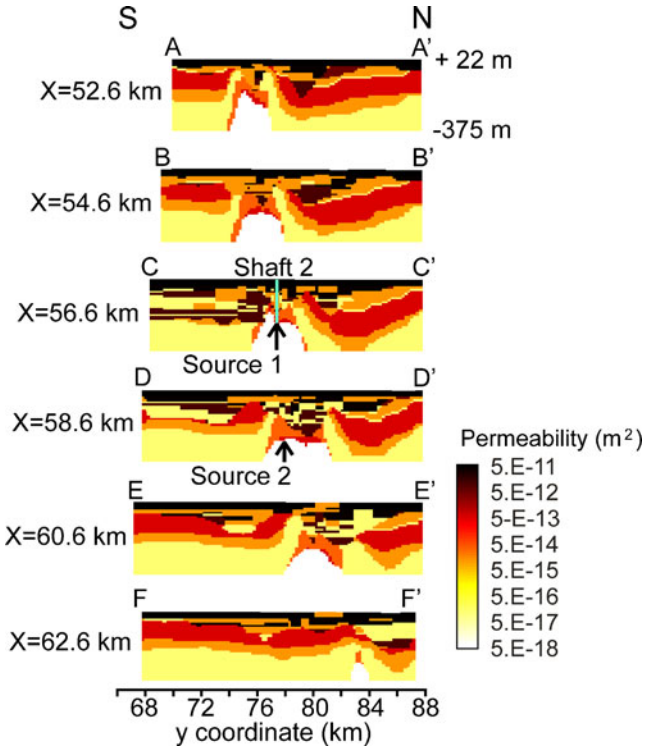

Fig. 6 Gorleben model. Vertical N–S sections showing rock permeabilities and the location of the radioactive sources 1 and 2 (the section traces are shown in Fig. 1)

multi-phase fluids in porous and fractured media. The program was developed by introducing reactive chemistry into the multi-phase flow code TOUGH2 (Pruess et al. 1999). The governing equations are discretised using integral finite difference for space and fully implicit first-order finite difference in time. The simulations are performed with the ECO2 module, which treats the aqueous phase as a mixture of water and salt.

The one-phase scenario is calculated with TOUGH2-MP, the parallel version of the TOUGH2 code (Zhang et al. 2008). The EOS7R module is used, which calculates the transport of a parent radionuclide and a daughter radionuclide. The aqueous phase is treated as a mixture of water and brine.

The main justification for using the TOUGH2 family of codes is the wide range of functions provided by its various modules. Alternative software for one-phase variable-salinity simulations is NAMMU, which calculates the transport of parent and daughter radionuclides (Serco 2003), and SUTRA-MS, which calculates single-chain radionuclides only (Hughes and Sanford 2004). Two-phase zero-salinity problems can be calculated with FLOTRAN (Lichtner 2007) or its parallel version PFLOTRAN (Mills et al. 2007). Although the software is not suitable for variable-salinity calculations, it is useful for inter-code comparisons under idealised zero-salinity conditions.

Methodology

The simulations are performed with variable salinity but isothermally. This is justified because density variations caused by temperature changes (8–22°C) are relatively small with respect to density variations caused by salinity changes (0–0.26 mass fraction salt) as well as simplifications and uncertainties related to calibrating a variable-density model.

The initialisation of the isothermal model is performed in two steps. During a short preliminary run, hydrostatic conditions are implemented using an initial pressure of 10^5 Pa, zero salinity, a permeability of 10^{-12} m^2 for all hydrostratigraphic units and porosities of case 1 (Table 2). This is followed by a second step with permeabilities of case 1 (Table 2), zero salinity in all model cells except the large-volume elements (10^{14} m^3) of the rock salt unit and the bottom layer, which have an initial salinity of 0.25 (mass fraction salt). Based on these boundary conditions, the diffusivity of salt is estimated in a trial-and-error procedure. A reasonable agreement between observed values (Klinge 1994; Klinge et al. 2007) and simulated values at the end of the 100,000-year initialisation period is obtained with a diffusivity of 10^{-7} m^2/s (Fig. 8). This optimised salinity distribution is in a quasi-steady state, i.e., it is maintained with insignificant variations throughout the following 2,000,000-year simulation period. A lower diffusivity (e.g. 10^{-9} m^2/s corresponding to free-water diffusivity) or a lower initial salinity (<0.25 mass fraction salt) would result in a less suitable density distribution, which would be characterised by relatively gentle vertical gradients. Note that the model is not a realistic simulation of the diffusive transport of salt but a realistic simulation of flow driven by density contrasts. The diffusivity is one of the parameters that is used to achieve a quasi-steady state close to the actual density distribution.

In a second initialisation run, a test was conducted to see whether the results could be improved if the permeabilities of the Quaternary and Tertiary units of case 2 (Table 2) were used instead of those of case 1. The permeability was varied in intervals of half an order of magnitude within the intervals specified in Table 2. The porosity, which has relatively little influence, is set at 0.3 for sandy units and 0.1 for silt/clay units or 0.2 for all units. The outer lateral boundaries are either closed (element volume <10^6 m^3) or open (element volume >10^6 m^3).

In addition, two sets of parameters that have been used in previous simulations were tested. These are cases 3 and 4, which have a salt diffusivity of 10^{-9} m^2/s, hydraulic properties shown in Table 2, closed lateral boundaries and a closed bottom boundary except for a section with a concentrated-brine Dirichlet boundary at the contact with the salt dome. Case 3 (after Keesmann et al. 2005) yields a salinity distribution that is both far from steady-state and far from agreement with observed values even after a 2-million-year initialisation period. Case 4 (after Klemenz et al. 1998) produced convergence problems and could not

 DOI 10.1007/s10040-011-0825-z

Table 2 Saturated hydraulic properties of rocks of the Gorleben model

Symbol	Rock	Case 1		Case 2		Case 3		Case 4	
		Permeability (m^2)	Porosity (−)	Permeability (m^2)	Porosity (−)	Permeability (m^2)	Porosity (−)	Permeability (m^2)	Porosity (−)
Quaternary									
qN	Holocene, Weichsel glacial (sand)	5×10^{-11}	0.3	10^{-13}-10^{-11}	0.2–0.3	10^{-12}	0.2	10^{-11}	0.2
qsS	Saale glacial (sand)	4×10^{-11}	0.3	10^{-13}-10^{-11}	0.2–0.3	10^{-12}	0.2	10^{-13}	0.2
qsU	Saale glacial (silt, clay, drift marl)	1×10^{-14}	0.15	10^{-15}-10^{-13}	0.1–0.2	10^{-14}	0.2	10^{-16}	0.2
qhol	Holstein interglacial (silt, clay)	1×10^{-16}	0.03	10^{-17}-10^{-15}	0.1–0.2	10^{-16}	0.2	10^{-16}	0.2
qLS	Elster glacial/Lauenburger-Ton-Komplex (sand)	1×10^{-11}	0.3	10^{-13}-10^{-11}	0.2–0.3	10^{-12}	0.2	10^{-11}	0.2
qLT	Elster glacial/Lauenburger-Ton-Komplex (clay, silt)	1×10^{-16}	0.03	10^{-17}-10^{-15}	0.1–0.2	10^{-16}	0.2	10^{-16}	0.2
qeS	Elster glacial (excluding Lauenburger-Ton-Komplex) (sand)	1×10^{-11}	0.3	10^{-13}-10^{-11}	0.2–0.3	10^{-12}	0.2	10^{-11}	0.2
qeU	Elster glacial (excluding Lauenburger-Ton-Komplex) (silt, drift marl)	1×10^{-14}	0.15	10^{-15}-10^{-13}	0.1–0.2	10^{-14}	0.2	10^{-16}	0.2
qpe	Bavel-Cromer-Komplex (silt)	1×10^{-14}	0.15	10^{-15}-10^{-13}	0.1–0.2	10^{-14}	0.2	10^{-16}	0.2
qme	Menap glacial (sand)	1.5×10^{-11}	0.3	10^{-13}-10^{-11}	0.2–0.3	10^{-12}	0.2	10^{-11}	0.2
Tertiary/Cretaceous/Zechstein									
tmiBS2	Lower Miocene/Obere Braunkohlensande (sand)	5×10^{-12}	0.3	10^{-13}-10^{-11}	0.2–0.3	10^{-12}	0.2	10^{-12}	0.2
tmiHTU	Lower Miocene/Hamburger-Ton-Komplex (silt, clay, sand)	1×10^{-14}	0.15	10^{-15}-10^{-13}	0.1–0.2	10^{-14}	0.2	10^{-16}	0.2
tmiHTT	Lower Miocene/Hamburger-Ton-Komplex (clay, silt)	1×10^{-16}	0.03	10^{-17}-10^{-15}	0.1–0.2	10^{-16}	0.2	10^{-16}	0.2
tmiBS1	Lower Miocene/Untere Braunkohlensande includ. Neochat (sand, silt)	5×10^{-13}	0.3	10^{-13}-10^{-11}	0.2–0.3	10^{-12}	0.2	10^{-12}	0.2
toloE	Upper Oligocene/Eochat (clay, silt)	1×10^{-14}	0.15	10^{-15}-10^{-13}	0.1–0.2	10^{-14}	0.2	10^{-16}	0.2
tolu	Lower Oligocene/Rupelton (clay, silt)	1×10^{-16}	0.03	10^{-17}-10^{-15}	0.1–0.2	10^{-16}	0.2	10^{-16}	0.2
teo + tpa	Eocene, Paleocene (clay, silt, sand)	3×10^{-14}	0.15	10^{-15}-10^{-13}	0.1–0.2	10^{-14}	0.2	10^{-16}	0.2
kro	Cretaceous (limestone, marlstone, sand)	1×10^{-14}	0.15	10^{-15}-10^{-13}	0.1–0.2	10^{-14}	0.2	10^{-16}	0.2
c	Caprock (former Zechstein salt)	5×10^{-13}	0.3	10^{-15}-10^{-13}	0.1–0.2	10^{-12}	0.2	10^{-12}	0.2
z	Zechstein salt	1×10^{-18}	0.1	10^{-18}	0.1	10^{-18}	0.1	10^{-18}	0.1

complete a 100,000-year initialisation run. In summary, cases 2–4 yielded results that proved to be inferior to those obtained with case 1. Therefore, only case 1 is used for the subsequent fixed-head simulations (base case and sensitivity cases A and B). It was found not to be necessary to perform an additional calibration for the transient head simulation (sensitivity case C). The effects on salinity distribution caused by changing the head are very minor in comparison to the effects caused by changing the diffusivity of salt or the initial salinity of the boundary cells.

The initial gas saturation is zero in all cells. The parameters for the capillary-pressure function of Van Genuchten (1980) are those for the Apache Leap tuff reported by Rasmussen (2001). The relative permeability of gas and liquid are calculated with the function of Corey (1954; quoted by Brooks and Corey 1964).

TOUGHREACT allows for injection of a single non-condensable gas, which is hydrogen in the case of the present study. Other gaseous species are introduced as secondary species via the corresponding

Table 3 Saturated hydraulic properties of structural materials of the Gorleben model

Material	Base Case		Case A		Case B	
	Permeability (m^2)	Porosity (−)	Permeability (m^2)	Porosity (−)	Permeability (m^2)	Porosity (−)
Backfill of Shaft 2	1×10^{-12}	0.3	2×10^{-12}	0.3	3×10^{-12}	0.3
Wall of Shaft 2	1×10^{-16}	0.1	1×10^{-16}	0.1	1×10^{-16}	0.1

 DOI 10.1007/s10040-011-0825-z

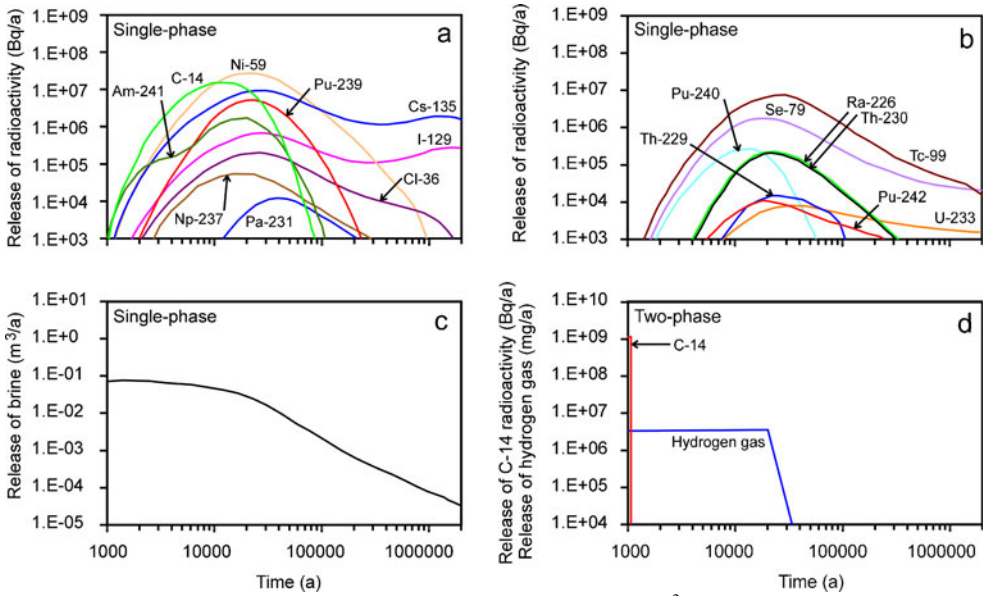

Fig. 7 Gorleben model. **a–c** The near-field release of radionuclides (Bq/a) and brine (m^3/a) from year 1,000 to year 2,000,000 after closure of the repository for the one-phase scenario. **d** The near-field release of hydrogen gas (mg/a) and C-14 (Bq/a) for the two-phase scenario

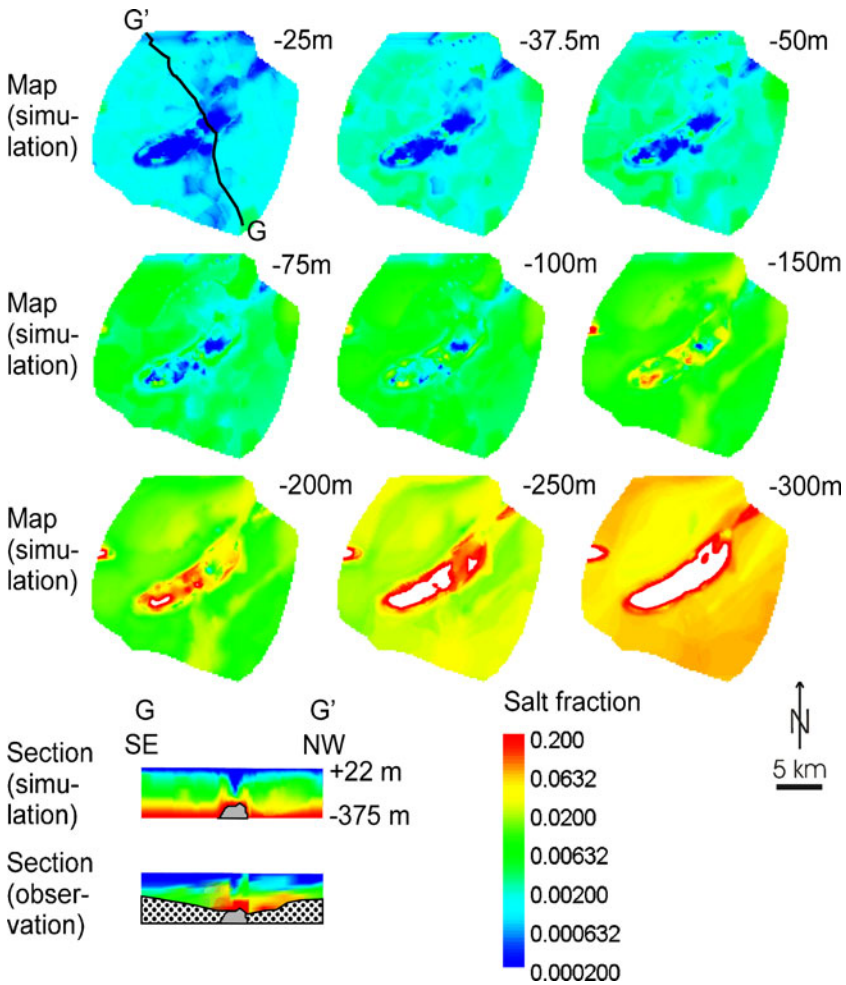

Fig. 8 Gorleben model. Maps with the simulated salinity (mass fraction salt) of the layers at −25, −37.5, −50, −75, −100, −150, −200, −250, and −300 m. SE–NW sections (G–G') are projected onto a vertical plane orientated S–N (vertical exaggeration ratio 12:1): simulated salinity (*grey* = salt dome) and observed salinity (*grey* = salt dome; *dotted pattern* = missing values)

 DOI 10.1007/s10040-011-0825-z

primary liquid species according to a dissociation reaction such as

$$HCO_3^- + H^+ = CO_{2(gas)} + H_2O. \quad (2)$$

The primary species are HCO_3^-, H^+ and $O_{2(aq)}$. The secondary species are $CO_{2(gas)}$, $CH_{4(gas)}$, $CH_{4(aq)}$, $CO_{2(aq)}$ and CO_3^{2-}. The initial and boundary solutions have a H^+ activity of 10^{-7} and an $O_{2(aq)}$ activity of 10^{-67}. The source for the two-phase model is the near-field release shown in Figure 7d. Hydrogen gas is injected into the primary central cell of shaft 2 on the −237.5-m level, whereas a boundary solution with HCO_3^- is injected from a secondary boundary cell that is connected to this primary cell (source 1; Fig. 6). Unfortunately, the different injection processes influence each other. The important variables are the length of the injection period for the boundary solution and the volume of the boundary cell. By trial-and-error, a volume of 100 m^3 was found to cause the least interference for the 100-year injection period.

The one-phase transport of radionuclides that do not partition into a gas phase is calculated with TOUGH2-MP. Initial conditions and boundary conditions are identical to those of the TOUGHREACT simulations except that salt fraction is converted to brine fraction. The source for the one-phase model is the near-field release of radionuclides (Figs. 7a and b) injected at the borehole location GoHy3020 on the −250-m level (source 2; Fig. 6). As opposed to the TOUGHREACT code, the TOUGH2-MP code uses idealised radionuclides without mass; i.e., there is no interference with the thermodynamic conditions of the remaining system.

Simulated radionuclide transport and radioactive dose

The simulation period is from year 1,000 to year 2,000,000 for 20 radionuclides (Table 1) in the single-phase scenario and from year 1,000 to year 8,000 for C-14 in the two-phase scenario. The relevant model depth for simulating the biosphere is the −37.5-m level; this is approximately the limit between freshwater and saline water (1 g/L salt), and wells that reach this level are assumed to supply the contaminated water in the biosphere model. The major paths to the exposed individual are the consumption of contaminated drinking water and consumption of plants that are watered with contaminated water, as well as the consumption of milk and meat from cattle that is watered with contaminated water (Keesmann et al. 2005).

The peak values at the −37.5-m level are 6.3×10^{-8} Bq/L (becquerel per litre) for the single-phase scenario and 1.1×10^{1} Bq/L for the base case of the two-phase scenario (Fig. 9). These values are reached in the year 2,000,000 (end of the simulation period) and in the year 7,000 for the one-phase and two-phase scenario, respectively.

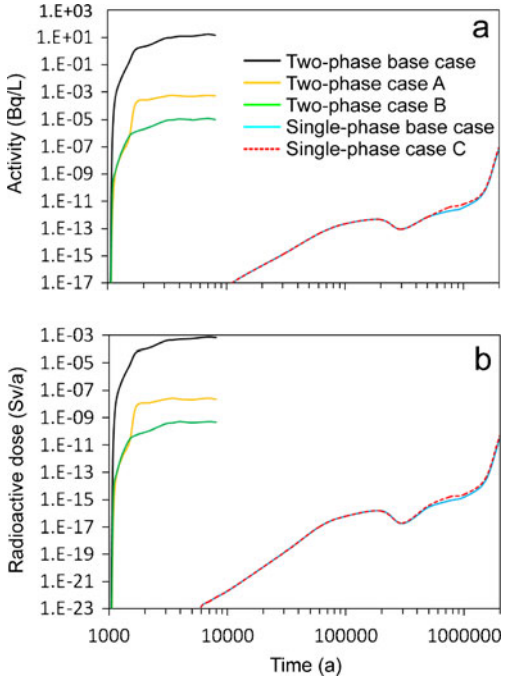

Fig. 9 Gorleben model. Peak values of **a** radioactivity (Bq/L) and **b** radioactive dose (Sv/a) on the −37.5-m level. Two-phase scenario with base case (shaft 2 with a permeability of 10^{-12} m^2), *case A* (2×10^{-12} m^2) and *case B* (3×10^{-12} m^2). One-phase scenario with base case (fixed head) and *case C* (transient head)

The calculation of the radioactive dose is based on dose conversion factors (DCFs; Keesmann et al. 2005). The annual dose D_D (Sv/a; sievert per year) is calculated according to the equation

$$D_D = \sum X_i C_i \quad (3)$$

where X_i is the concentration (Bq/L) of the radionuclide i and C_i is the DCF (Sv/a:Bq/L) of the radionuclide i.

The peak dose on the −37.5-m level is 3×10^{-11} Sv/a for the single-phase scenario and 8×10^{-4} Sv/a for the base case of the two-phase scenario. The relatively simple shape of the radioactive plume in the one-phase scenario (Fig. 10) confirms previous qualitative predictions on groundwater flow in the N–NE section of the Gorlebener Rinne (paleo-channel filled with Quaternary sediments; Klinge et al. 2007). In addition, there is a S branch, which is partly due to the water flow in the S section of the Gorlebener Rinne. This branch could not be predicted with the available qualitative methods, which relied on the interpretation of salinity distribution, hydraulic gradient and permeability (Klinge et al. 2007).

Sensitivity analysis

The permeability of the sedimentary cover rocks (Tertiary and Quaternary) and the structural material of shaft 2 are variables that strongly influence the

DOI 10.1007/s10040-011-0825-z

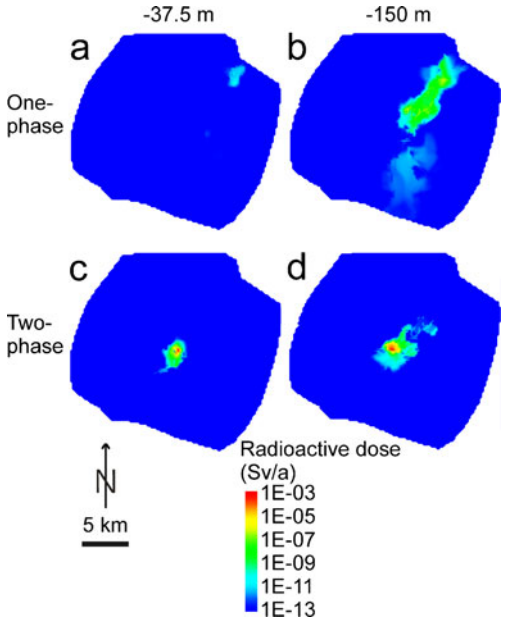

Fig. 10 Gorleben model. Maps with radioactive dose (Sv/a) in the simulation year 2,000,000 for the base case of the *one-phase* scenario and year 7,000 for the base case of the *two-phase* scenario. **a** −37.5–m layer with one-phase scenario. **b** −150-m layer with one-phase scenario. **c** −37.5-m layer with two-phase scenario. **d** −150-m layer with two-phase scenario

transport of radionuclides. Unfortunately, sensitivity tests with rock permeabilities are not feasible because rock permeability and salinity (i.e. fluid density) are strongly correlated (see Methodology). Nevertheless, the permeability of the structural material used for sealing shaft 2 can be varied without any significant influence on salinity distribution.

As opposed to one-phase simulations, two-phase simulations are very time-consuming (more than four weeks computing time). Therefore, only two sensitivity cases are calculated for the whole length of the simulation period (7,000 years). Increasing the permeability of the backfill of shaft 2 by a factor of 2 (case A) or a factor of 3 (case B) results in a decrease of the radioactive dose to values below the regulatory limit (10^{-4} Sv/a; Fig. 9). Scoping calculations over shorter periods show that decreasing the permeability would have the opposite effect.

The effect of changing head conditions is simulated for the one-phase scenario. Replacing the fixed head of the base case by a transient head (see section Geometry of the models in the preceding) results in an increase of the radioactive dose up to a factor of 2 (case C; Fig. 9).

Discussion and conclusions

The risk assessment for a nuclear waste repository in the Gorleben salt dome is a highly complex task. Although this study only addresses a subproblem, it has important implications for a safety analysis. Two major themes that have been neglected in the past due to computational restrictions need careful consideration in the future. These are the transport of radionuclides in a liquid phase driven by density contrasts in three dimensions and the transport of radionuclides in two phases (gas and liquid).

This report does not present probabilistic risk assessments but deterministic cases with sensitivity tests. Thus, the question arises for which type of assessment these cases are representative. The single-phase near-field scenario is based on 2,000 m^3 of brine dissolving the radioactive waste in defective canisters. It is implicitly conceived as a pessimistic case (Keesmann et al. 2005) and probably can be considered as being pessimistic at the present state of knowledge.

The two-phase scenario implies a relatively small volume of brine (1,000 m^3) causing the corrosion of a relatively small fraction of the waste containers (0.6%). According to the latest estimates, the volume of brine pockets expected to be present in the repository is several thousand m^3 (Bundesamt für Strahlenschutz 2010). These estimates do not account for the humidity of crushed-salt backfill, the brine content of which corresponds to about 1 wt% liquid (Stührenberg 2010). Equally important, the estimates do not account for microscopic brine inclusions in solid rock salt (<0.2 wt %). The inclusions tend to migrate within rock-salt crystals towards the region with higher temperature (Roedder 1984, 1990). Thus, the canisters containing heat-producing waste are the target for brines released from these minute occurrences.

The conditions of gas release constitute a great source of uncertainty. There is the possibility of unsteady or explosive release of hydrogen gas transporting short-lived radionuclides (Schulze 2002). Furthermore, the permeability of the backfill of the shaft, through which the gas is assumed to flow, has a strong influence on the performance of the repository.

For a steady (non-explosive) gas release, a backfill permeability of 10^{-12} m^2 results in a radioactive dose of 0.8 mSv/a (millisievert per year) for C-14, which strongly partitions into the gas phase. A higher permeability would decrease the radioactive dose of C-14 to values below the regulatory limit (0.1 mSv/a) but would increase the risk of contamination by radionuclides that predominate in the liquid phase. A relatively high permeability favours the flow of liquid with respect to the flow of gas, whereas a relatively low permeability has the opposite effect. A low permeability is the appropriate safety concept for a one-phase scenario (only liquid transport); however, a high permeability is the appropriate concept for a two-phase scenario (gas-dominated transport). As both scenarios deserve equal consideration in a risk analysis, there is a typical conflict of targets. A low permeability is an optimistic scenario if minimal contaminant-transport in the liquid phase is the target

 DOI 10.1007/s10040-011-0825-z

or a pessimistic scenario if minimal contaminant-transport in the gas phase is the target (and vice versa).

Acknowledgements This study was carried out with the help of the staff of the Bundesanstalt für Geowissenschaften und Rohstoffe, Hannover, Germany (BGR) but it did not obtain financial support from the BGR or any other organisation. Above all, the report benefited from advice given by P. Vogel (BGR). His experience with alternative software (SUTRA family of codes) proved to be very valuable.

References

Beushausen M, Ludwig R (1990) Hydrogeologische Gliederung der oberoligozänen und miozänen Schichten [Hydrogeological classification of the upper Oligocene and Miocene strata]. Report archive no. 106036, Bundesanstalt für Geowissenschaften und Rohstoffe, Hannover, Germany

Bornemann O, Behlau J, Fischbeck R, Hammer J, Jaritz W, Keller S, Mingerzahn G, Schramm M (2008) Standortbeschreibung Gorleben, Teil 3: Ergebnisse der über- und untertägigen Erkundung des Salinars [Description of the Gorleben site, part 3: results of the surface and underground exploration of the salt formation]. Geol Jahrb C73:5–211

Brooks RH, Corey AT (1964) Hydraulic properties of porous media. Hydrology Papers 3, Colorado State University, Fort Collins, CO, pp 1–27

Bundesamt für Strahlenschutz (2010) Lösungsvorkommen im Salzstock Gorleben [The occurrence of fluids in the Gorleben salt dome]. http://www.bfs.endlager/gorleben/loesungen_salzstock.html. Cited on 3 June 2010

Corey AT (1954) The interrelation between gas and oil relative permeabilities. Producer's Monthly, vol 19, no. 1, November 1954 (quoted by Brooks and Corey 1964)

GSF (2006) Deckgebirgsmodellierung Phase IV: Grundwasserbewegungen im Deckgebirge des Standortes Asse [Cover rock modelling phase IV: Groundwater movements in the cover rock of the Asse site]. GSF Forschungszentrum für Umwelt und Gesundheit, München, Germany

Hughes JD, Sanford WE (2004) SUTRA-MS: a version of SUTRA modified to simulate heat and multiple-solute transport. US Geol Surv Open-File Rep 2004–1207, 141 pp

Javeri V (2006) Three-dimensional analyses of coupled gas, heat and nuclide transport in a repository including rock salt convergence. Proceedings, TOUGH Symposium 2006, 15–17 May 2006, Lawrence Berkeley National Laboratory, Berkeley, CA, 9 pp

Johns RT, Rivera A (1996) Comment on "Dispersive transport dynamics in a strongly coupled groundwater-brine flow system" by Curtis M. Oldenburg and Karsten Pruess. Water Resour Res 32:3405–3410

Keesmann S, Nosek U, Buhrmann D, Fein E, Schneider A (2005) Modellrechnungen zur Langzeitsicherheit von Endlagern in Salz- and Granit-Formationen [Model calculations for the long-term safety of repositories in salt and granite formations]. Report GRS-206, GRS, Braunschweig, Germany

Klemenz W, Rivera A, Wollrath J, Genter M (1998) Three-dimensional coupled groundwater movement and salt transport calculations as part of the safety assessment of the Gorleben repository, Germany. Proceedings DisTec'98, 9–11 September 1998, Hamburg, Germany, pp 591–596

Klinge H (1994) Zusammenfassende Bearbeitung der chemischen und isotopengeochemischen Zusammensetzung der Grundwässer im Deckgebirge des Salzstocks Gorleben [Summary of the investigations on the chemical and isotopic composition of the groundwater in the cover rock of the Gorleben salt dome]. Report archive no. 0111699, Bundesanstalt für Geowissenschaften und Rohstoffe, Hannover, Germany

Klinge H, Margane A, Mrugalla S, Schelkes K, Söfner B (2001) Hydrogeologie des Untersuchungsgebietes Dömitz-Lenzen [Hydrogeology of the Dömitz-Lenzen exploration area]. Report archive no. 0121207, Bundesanstalt für Geowissenschaften und Rohstoffe, Hannover, Germany

Klinge H, Boehme J, Grissemann C, Houben G, Ludwig R, Rübel A, Schelkes K, Schildknecht F, Suckow A (2007) Standortbeschreibung Gorleben, Teil 1: Die Hydrogeologie des Deckgebirges des Salzstocks Gorleben [Description of the Gorleben site, part 1: hydrogeology of the cover rock of the Gorleben salt dome]. Geol Jahrb C71:5–147

Konikow LF, Sanford WE, Campbell PJ (1997) Constant-concentration boundary condition: lessons from the HYDROCOIN variable-density groundwater benchmark problem. Water Resour Res 33:2253–2261

Köthe A, Hoffmann N, Krull P, Zirngast M, Zwirner R (2007) Standortbeschreibung Gorleben, Teil 2: Die Geologie des Deck- und Nebengebirges des Salzstocks Gorleben [Description of the Gorleben site, part 2: the geology of the cover rock and country rock of the Gorleben salt dome]. Geol Jahrb C72:5–201

Lichtner PC (2007) FLOTRAN user's manual: two-phase non-isothermal coupled thermal-hydrologic-chemical (THC) reactive flow & transport code, version 2.0. Report LA-UR-01-2349, Los Alamos National Laboratory, Los Alamos, NM, pp 1–168

Ludwig R, Mandl J, Uhlig A (1989) Zwischenbericht über die Diskretisierung hydrogeologischer Strukturen im Bereich Gorleben [Interim report on the discretisation of hydrogeological structures in the Gorleben area]. Report archive no. 0105061, Bundesanstalt für Geowissenschaften und Rohstoffe, Hannover, Germany

Ludwig R, Schneider M, Sewing D (1993) Projekt Gorleben: Hydrogeologische Gliederung der quartärzeitlichen Schichtenfolge [Project Gorleben: Hydrogeological classification of the Quaternary strata]. Report archive no. 110256, Bundesanstalt für Geowissenschaften und Rohstoffe, Hannover, Germany

Ludwig R, Schelkes K, Vogel P, Wollrath J (2001) Implications of large-scale heterogeneities for hydraulic model studies at the potential site of a radioactive waste repository at Gorleben, Germany. Eng Geol 61:119–130

Mills RT, Lu C, Lichtner PC, Hammond GE (2007) Simulating subsurface flow and transport on ultrascale computers using PFLOTRAN. J Phys Conf Ser 78:1–7

NAGRA (2002) Project Opalinus Clay: safety report. NAGRA technical report 02–05, NAGRA, Wettingen, Switzerland

Nykyri M, Nordman H, Marcos N, Löfman J, Poteri A, Hautojärvi A (2008) Radionuclide release and transport - RNT-2008. POSIVA Report 2008–06, Olkiluoto, Finland, 164 pp

Oldenburg CM, Pruess K (1995a) Dispersive transport dynamics in a strongly coupled groundwater-brine flow system. Water Resour Res 31:289–302

Oldenburg CM, Pruess K (1995b) Strongly coupled single-phase flow problems: effects of density variation, hydrodynamic dispersion, and first order decay. Paper presented at the TOUGH Workshop '95, 20–22 March 1995, Earth Sciences Division, Lawrence Berkeley Laboratory, University of California, Berkeley, CA, 6 pp

Oldenburg CM, Pruess K, Travis BJ (1996) Reply to Comment on "Dispersive transport dynamics in a strongly coupled groundwater-brine flow system". Water Resour Res 32:3411–3412

Pruess K, Oldenburg C, Moridis G (1999) TOUGH2 user's guide, version 2.0. Earth Sciences Division, Lawrence Berkeley National Laboratory, University of California, Berkeley, CA, 198 pp

Rasmussen TC (2001) Pressure wave vs. tracer velocities through unsaturated fractured rock. In: Evans DD, Nicholson TF, Rasmussen TC (eds) Flow and transport through unsaturated fractured rock, 2nd edn. AGU Geophysical Monograph 42, AGU, Washington, DC, pp 45–52

Roedder E (1984) The fluids in salt. Am Mineral 69:413–439

Roedder E (1990) Formation, handling, storage and disposal of nuclear wastes. J Geol Educ 38:360–392

Saripalli KP, Serne RJ, Meyer PD, McGrail BP (2002) Prediction of diffusion coefficients in porous media using tortuosity factors based on interfacial areas. Ground Water 40:346–352

Schulze O (2002) Auswirkung der Gasentwicklung auf die Integrität geringdurchlässiger Barrieregesteine [Gas generation affecting the integrity of low-permeability barrier rocks]. Report archive no. 0122442, Bundesanstalt für Geowissenschaften und Rohstoffe, Hannover, Germany, 142 pp

Schwartz MO (2009) Modelling groundwater contamination above the Asse 2 medium-level waste repository, Germany. Environ Earth Sci 59:277–286

Schwartz MO (2010) Clearing out Asse 2. Nuclear Engineering International, July 2010. http://www.neimagazine.com/story.asp?storyCode=2057290. Cited 27 Dec 2011, pp 26–27

Serco (2003) NAMMU 7.2 user guide. Serco, Didcot, UK, 262 pp

SKB (2006) Long-term safety for KBS-3 repositories at Forsmark and Laxemar: a first evaluation. SKB technical report TR-06-09, Stockholm, Sweden, 620 pp

Storck R, Aschenbach J, Hirsekorn RP, Nies A, Stelte N (1988) PAGIS performance assessment of geological isolation systems for radioactive waste: disposal in salt formations. Office for Official Publications of the European Communities, Luxembourg, 788 pp

Stührenberg D (2010) Laborversuche an Versatzvarianten in der Oedometerzelle [Laboratory experiments with various backfill types in the oedometer cell]. http://www.geozentrum-hannover.de. Cited 3 June 2010

Suter D, Biehler D, Blasser P, Hollmann A (1998) Derivation of a sorption data set for the Gorleben overburden. Proceedings DisTec '98, 9–11 September 1998, Hamburg, Germany, pp 581–584

van Genuchten MT (1980) A closed-form equation for predicting the hydraulic conductivity of unsaturated soils. Soil Sci Soc Am J 44:892–898

Vogel P (2005) Orientierende 3-D-Grundwassermodellrechnungen auf den Strukturen eines hydrogeologischen Modells Gorleben [Scoping calculations for a hydrogeological 3-D model structure of the Gorleben area]. Report archive No. 0125865, Bundesanstalt für Geowissenschaften und Rohstoffe, Hannover, Germany, 70 pp

Vogel P, Schelkes K (1996) Influence of initial conditions and hydrogeological setting on variable density flow in an aquifer above a salt dome. Proceedings ModelCARE 96 Conference, Golden, CO, September 1996, IAHS Pub no. 237, IAHS, Wallingford, UK pp 373–381

Xu T, Sonnenthal E, Spycher N, Pruess K (2005) TOUGHREACT user's guide: a simulation program for non-isothermal multiphase reactive geochemical transport in variably saturated geologic media. Earth Sciences Division, Lawrence Berkeley National Laboratory, Berkeley, CA, 195 pp

Zhang K, Wu Y, Pruess K (2008) User's guide for TOUGH2-MP: a massively parallel version of the TOUGH2 code. Earth Sciences Division, Lawrence Berkeley National Laboratory, Berkeley, USA, 108 pp

 DOI 10.1007/s10040-011-0825-z